AERODYNAMIC SHAPE OPTIMIZATION STUDY OF DIFFUSER IN TURBULENT FLOW

Shlomy Shitrit[1]
RAFAEL, Advanced Defense Systems, Ltd., Haifa 31021, Israel

Diffusers are the integral parts of many engineering applications and flow systems. An improperly designed diffuser may cause flow separation and low efficiency. The following study presents an approach of a single-point aerodynamic shape optimization of diffusers in turbulent flow. The objective in this study is to maximize the pressure recovery by shaping the diffuser's geometry, taking into account geometrical and aerodynamic constraints. Mesh warping and geometry parametrization is accomplished by fitting the multi-block structured grid to a B-spline volumes and performing the mesh movements by using surface control points embedded with free-form deformation (FFD) volumes. The aerodynamic model solves the RANS equations with Spallart-Almaras turbulence model. A gradient based optimization algorithm is used with an adjoint method in order to compute the objectives and constraints derivatives with respect to the design variables. The single-point optimization simulation increased the pressure recovery coefficient by 12% using 46 design variables. The effect of varying the number of shape design variables is examined. Also, nearly identical configuration is obtained while starting the simulation with a deformed geometry, and the final optimized pressure recovery values differ by 0.8% only. The accuracy and scalability of the presented method make it possible perform shape design optimization for diffusers characterized with complicated geometries under various flow conditions.

Nomenclature

ρ	=	density, kg/m^3
u, v, w	=	velocity components, m/s
p	=	static pressure, Pa ; order of convergence
R	=	residual
Rey	=	Reynolds number
FFD	=	free form deformation
y+	=	yplus
Cp	=	pressure recovery coefficient
ncp	=	number of control points
ndv	=	number of design variables
GCI	=	grid convergence index
N	=	mesh size
H	=	inlet reference length, m
AR	=	outlet to inlet area ratio (length in 2D)
L	=	grid level

Subscripts

baseline	=	initial configuration
ref	=	reference value

[1] Research Engineer, CFD group, Aeronautical Systems, P.O. Box 2250; shlomy.shitrit@gmail.com

I. Introduction

The function of a diffuser is to convert translational kinetic energy into thermal energy as efficiently as possible. For example, the inlet to a jet engine is a diffuser regardless of the flight speed. Good engine performance requires a high pressure inside the combustor. For supersonic flight the inlet diffuser significantly slows the flow and raises the static pressure. In this case the diffuser is an essential integrated part since loss on stagnation pressure across a normal shock can be quite large. Such loss results in a reduced engine efficiency. The fact that the viscous boundary layer experiences an adverse pressure gradient in any diffuser represents a major difficulty. This adverse pressure gradient increases with the inlet Mach number, and finally can cause boundary layer separation from the wall. The separated flow acts as an effective wall which is "seen" by the external flow as a ramp. If the external flow is supersonic then the ramp causes a shock wave that further alters the overall flow field.

In well-designed diffusers the total pressure loss is minimal and the flow at the exit plane is uniform. There are engineering applications that short straight diffusers are demanded because of weight or limited volume considerations. The result may be large area ratio that may cause boundary layer separation and excessive total pressure loss. There are sophisticated techniques for reducing (or even avoiding) flow separation phenomenon, for example: guide vanes, boundary layer suction or blowing, and wall shaping. In this study we focus on the last technique since it directly manages with the flow separation problem and no special equipment is required.

The aerodynamic shape optimization, even for only a wing design, more than ten years ago has been a very difficult task. A typical aerodynamic optimization process requires a robust mesh warping method, grid parametrization, CFD solver, and optimization algorithm. The tremendous improvements in each of these fields in the last few years, and the fact that researches made them available as an open source tools, allow aerodynamicists in academy as well as in industry, actually perform an aerodynamic shape optimization and robustly explore a design space that perfectly fits the engineering requirements. These useful tools allow not only for improving existing designs, but also reach unconventional configurations with much improved performances.

Numerical optimization approaches are usually categorized to gradient-based method and gradient-free methods. The adjoint method for computing the gradients along with an optimizer that is the gradient-based is proven to be the most efficient method for large scale problems with hundreds of design variables [1] [2] [3]. Pironneau [4] first introduced the adjoint method for drag minimization problems, and then Jameson [5] extended to the aerodynamic optimization of the Euler flow in the late 1980's. Since then various researchers have applied this method within complex implementations for aerodynamic problems [6] [7] [8] [9] [10] [11].

Aerodynamic design optimization process is very sensitive to the starting design sometimes and requires trial and error to get a converged optimal design. Xialong et al. [12] addresses this need by developing ways to overcome robustness issues arising from mesh warping, shape parametrization and CFD solver. They demonstrated the NACA0012 and RAE-2822 airfoil benchmarks to show the dominant factors influence the convergence efficiency. In addition they solved a challenging aerodynamic shape optimization case that starts from a circle in order to test the framework robustness.

In recent years, aerodynamic shape optimization based on flow analysis is becoming popular among researchers. Most remarkable numerical studies on the optimization of 2D and conical diffusers for incompressible flow were published during the early 90^{th}. Svenning et al. [13] presented a quasi-analytical sensitivity analysis as an optimization tool for CFD problems. They

applied their method on a two-dimensional laminar flow diffuser by shaping the wall aiming to improve the pressure recovery (Cp). Only a minor Cp improvement was obtained (3%) compared to straight wall configuration.

Results derivative-based design optimization of turbulent subsonic diffusers was presented by Madsen et al. [14]. They considered the two mentioned approaches shaping the diffuser wall and using guide vanes. A marginal improvement was obtained for diffusers with small area ratio, and the pressure recovery of wide-angled diffusers substantially improved. Madsen et al. [15] also used the response function method to optimize a 2D diffuser. Their goal was to improve the pressure recovery by using two different wall profiles. A small gain in Cp values was obtained (around 1% only).

A variation formulation was derived by Cabuk and Modi [16] to determine the diffuser wall profile (with constant width and length) in order to get the maximum static pressure rise. Their method was applied on a 2D laminar diffuser for maximizing Cp. The performance of the optimized configuration improved dramatically compared to straight line diffuser with the same area ratio at several Reynolds numbers.

Wall shaping of a 2D diffuser for maximum Cp was studied by Lund et al. [17]. They used B-spline method to control the wall shape by using 5 control points moving vertically. Only a small improvement of Cp was obtained.

Dehghani et al. [18] studied the optimization of laminar flow diffusers by wall contouring with a given length ratio. The developed algorithm uses the commercial CFD software Fluent for the hydrodynamic analysis and employs surrogate modeling for the optimization process. The non-uniform rational basin splines (NURBES) are used to represent the diffuser's wall with three to nine design variables. The CFD analysis and the surrogate model have been combined for a fully automated operation using Matlab. The optimal design exhibits a reasonable performance improvement compared with the reference design. Another experience with the same diffuser baseline geometry is demonstrated in the present paper, inspired by Deghani et al [18].

The present paper demonstrates a modest experience and first steps done towards the construction of an aerodynamic shape optimization capability while applying the Adflow algorithm which is part of the MDO lab framework that made available as an open-source in the last year (2019-2020). A set of results are presented for a 2D diffuser. This is a Reynolds number constrained pressure recovery maximization problem. The tools used for this study are a subset of the multidisciplinary design optimization (MDO) framework of aerodynamic configurations (MACH) [19]. In the present study only the MACH's components relevant for aerodynamic shape optimization are used: CFD solver, mesh warping, geometric parametrization and optimization algorithm. The availability of these open-source tools and benchmarks enabled further studies in CFD-based aerodynamic design optimization. This paper is organized as follows. The introduction of the optimization tools are briefly described in Section 2. Sections 3 and 4 describe the optimization results of a 2D diffuser.

II. Methodology

The drag minimization of the problems presented in this work is obtained by using a CFD solver coupled with and adjoint solver to compute the objectives and constraints sensitivities, a robust

mesh warping routine and a gradient based optimizer. The pyGeo routine used for geometric manipulation, iDWarp for mesh deformation, Adflow as the flow solver and SLSQP as the numerical optimization algorithm.

A. CFD solver

The CFD solver used in this research is three dimensional multi-block structured finite volume solver (SUmb). The parallel implicit solver is capable of solving the Euler and Reynolds averaged Navier-Stokes (RANS) equations (steady and unsteady) [20]. The discretization of the governing equations is done by a finite volume approach with a central formulation over structured meshes. The convective terms are computed by the Jameson-Schmidt-Turkel [21] scheme using flux splitting upwind scheme with Van-Albeda limiter. Viscous fluxes are computed to second order accuracy using a central difference approach. The residual smoothing is made by employing an explicit 5th order Runge-Kutta algorithm employing well known steady-state acceleration techniques including local time stepping and implicit residual smoothing. For RANS analysis the turbulent equations are solved in coupled fashion using diagonally-dominant alternating direction implicit (DD-ADI) scheme. In order to improve convergence, the solver is also equipped with a diagonallized ADI method for the mean flow equations and Newton-Krylov (NK) solver. The computational coordinates is x, y and z axes, while x in the stream-wise direction, y vertical, and z span-wise. The origin is located at the inlet bottom corner.

The steady state mean flow equations discretized using a finite volume cell centered formulation , yielding a set of ordinary differential equations that can be written as follows: $R(w_{ijk}) = 0$, where w is a vector of the mean flow varibales: $w = \{\rho, \rho u, \rho v, \rho w, \rho E\}^T$, and R is the residual obtained by evaluating the sum of integral fluxes of the governing equations, to the second order of accuracy.

B. Free Form Deformation (FFD) and mesh warping

The geometry parametrization is done by the FFD approach [22]. In this approach the geometry is located inside a B-Spline control volume while the coordinates are mapped to the external surface of the volume by Newton search algorithm. All the geometric modifications are made on the external surfaces of the FFD volume. Any modification of the FFD boundaries indirectly modifies the internal geometry. The main assumption of this approach is a constant topology throughout the optimization process.

After the FFD volumes modify the geometry during the optimization process, the mesh must be warped in order to solve the flow field for the modified geometry. In this work the algebraic mesh perturbation scheme is used, which is developed by Kenway et al. [22].

C. Optimization algorithm

In this research work the SLSQP (sequential least square programming) optimization algorithm is applied. It is part of the pyOpt framework Perez [23] which is an open source software. The algorithm SLSQP [24] is evolved from the least squares solver [8]. It uses a quasi-Newton Hessian approximation and an L1-test function in the line search algorithm.

III. Problem formulation

The optimization problem presented here is the pressure recovery maximization of a generic plane symmetric diffuser in viscous flow. The aim is to determine the optimum shape of the diffuser's upper wall in a way that increases the pressure recovery and decrease the pressure loss.

The diffuser inlet width is H, the length is 3H, and constant size of inlet and outlet section as 0.75H and 6H, respectively. These geometry parameters are constant and serves as part of the problem constraints. The inlet boundary condition is BCInflowSubsonic (according to CGNS format), namely, constant values of total pressure and temperature, and axial velocity direction. The Outflow boundary condition is a constant static pressure. The pressure rise depends upon the flow rate through the diffuser, which is characterized by the Reynolds number. So, theoretically we would like to define an axial flow direction through the inlet, characterized by a constant Reynolds number, which means – a constant mass flow rate. However, since such a boundary condition is not available in the current CGNS framework, the inlet constant mass flow rate is achieved by using the inlet Reynolds number as a constraint and the outlet static pressure as a design variable. By varying the outlet static pressure conditions, the desired Reynolds number is obtained. In this way the outlet static pressure has two functions – one as a boundary condition (outlet condition) and second as a design variable. The upper wall is a no-slip wall, and the centerline (bottom line) has a symmetry boundary condition.

A uniform compressible flow with a density of 1.225Kg/m3 and Reynolds number of $Rey = 10^5$ enters the domain (from left to right). The Reynolds number is based on the diffuser inlet length, H, as the reference length. A non-dimensional pressure recovery is defined by a pressure coefficient Cp as,

$$C_p = \frac{p_{outlet} - p_{inlet}}{{}^1/_2 \rho {u_{inlet}}^2}$$

The aerodynamic optimization problem formulation is summarized in Table 2. In order to increase the flexibility of the optimization problem, the diffuser outlet section is not fixed, and the aspect ratio (AR-outlet length divided by the inlet length H) is allowed to vary in the range of $1.8 < AR < 4$. Namely, the upper wall of the 6H outlet section (FFD-3) is allowed to move as a solid body in the y-direction only. The design space includes control points along the upper wall, which successively doubled beginning with 3 points up to maximum of 24 control points. The first control point (common to FFD-1 and FFD-2) is fixed at the inlet and the last control point (the first point in FFD-3) can move only in y-direction, the total number of the design variables involved are: 8, 20, 44, 92. In order to control the upper wall shape, the coordinates of each control point are constrained by the upper and lower bounds (see Table 2). The bounds values are FFD-mesh dependent, and are predefined according to the interval between the FFD-2 control points. The lower and upper bounds for the different cases are summarized in Table 2.

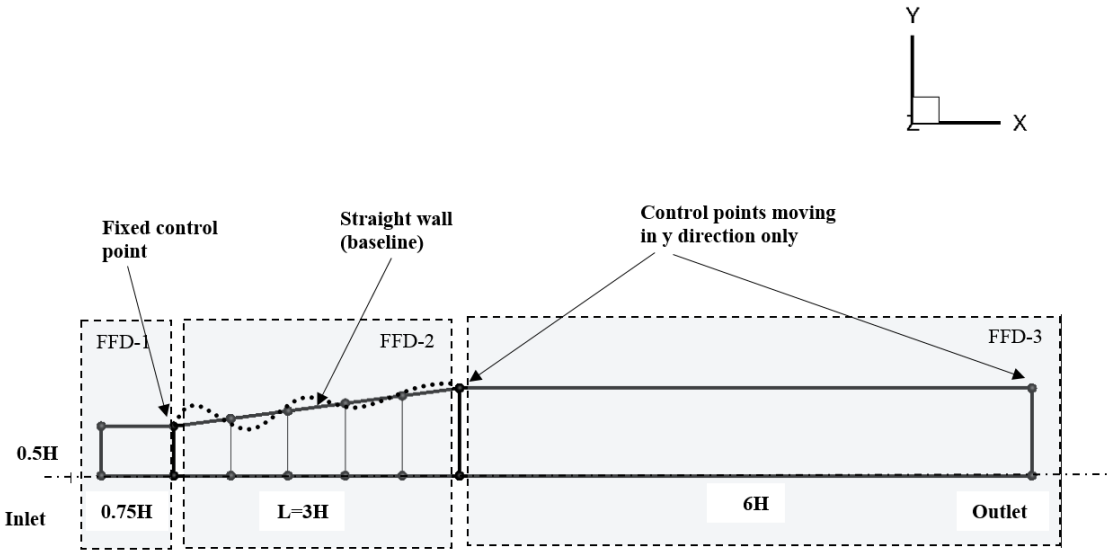

Figure 1: A symmetric diffuser model, including the FFD blocks.

Table 1: Control points and design variables

Control points	3	6	12	24
Design variables	8	20	44	92

Table 2: The diffuser problem statement

	Name	Quantity	Lower value	Upper value
Objective	Minimum (1-Cp)	1	-	-
Design variables	Ptot(inlet)	1	95000	105000
	x,y directions	46	-	-
Constraint	Rey	1	100000	100000

IV. Grid convergence study

The grid topology includes 4160 (level L1) cells. The minimum cell size close to the boundary is $3 * 10^{-6}\, m$, reaching $y^+ \approx 1$. Grid convergence study was conducted while refining the grid in x, y directions. The aerodynamic coefficients results of three different grid refinement levels are collected in
Table 3.
Grid convergence study has been made based on the Grid Convergence Index (GCI) method, for examining the spatial convergence of CFD simulations presented in the book by Roache [25]. Roache suggests a GCI to provide a consistent manner in reporting the results of grid convergence studies and also an error band on the grid convergence of the solution. This approach is also based upon a grid refinement estimator derived from the theory of Richardson Extrapolation [7]. The GCI on the fine grid is defined as: $GCI_{fine} = \frac{F_s}{r^p - 1}$ where F_s is a factor of safety (recommended to be $F_s = 1.25$ for comparisons over three or more grids). The GCI for coarser grid is defined as $GCI_{fine} = \frac{F_s r^p}{r^p - 1}$, while each grid level yield solutions that are in the asymptotic range of convergence for the computed solution. The parameter p is the order of convergence (here a second order accuracy is involved, so theoretically the maximum value is p=2), and r is the effective grid ratio: $r = \left(\frac{N_1}{N_2}\right)^{1/d}$ where N is the total number of grid points in executive grid levels, and d is the flow dimension. Since the grid was adapted only in two directions (chordwise and normal directions) and in spite of the fact that we actually solve 3D

problem, a d=2 is defined. The asymptotic range of convergence can be checked by observing the two GCI values as computed over three grids, $GCI_{23} = r^p GCI_{12}$, while values approximately unity indicates that the solutions are within the asymptotic range of convergence. For this purpose three levels of grid refinement have been checked to assess the effect on the numerical accuracy, while the total grid cells number: $L0 = 5440$ cells, $L1 = 4160$ cells and $L2 = 1536$ cells. The grids generated with clustering cells near the walls results in $y^+ \approx 1$.
The GCI values including the asymptotic range of convergence and an estimation of the pressure recovery coefficient values at zero grid spacing are detailed in Table 4. Based on this study we can say, for example, that Cp is estimated to be $Cp = 0.6238$ with an error band of 1.66%. The grid resolution studies confirmed that the computed pressure recovery coefficient is grid converged.

Table 3: Grid convergence study

Grid level (cells number)	Cp	Y+
L0-5440	0.6156	1
L1-4160	0.6046	6
L2-1536	0.5787	10

Table 4: Pressure recovery coefficient in the grid convergence study

	Grid level	Grid ratio, r	GCI [%]	Richardson extrapolation
C_p	L0	1	-	0.6238
	L1	1.15	1.660	-
	L2	1.53	0.294	-

V. Optimization results

Three aerodynamic optimization cases are involved here, and the details are presented in Table 5. Before optimizing the upper wall shape and in order to find the best straight wall diffuser, a preliminary run is performed (case1). For this purpose, the design variables are the FFD-3 upper control points which allowed to move in the y-direction only, and in range of $1.8 < AR < 4$. By varying the inlet total pressure, the desired $Rey = 10^5$ at the inlet is reached. In the second case the upper wall optimization shape is performed while varying the FFD-2 control points in x and y directions. The outlet area is also changeable according to the AR bounds. In order to verify that the optimized diffuser shape obtained in case 2 is the global maximum (in terms of Cp), and in order to explore the multi-modality of the single-point aerodynamic shape optimization, the optimization process is started from a different geometry. In the third case the starting point for the optimization process is a deformed geometry, characterized by a perturbed upper wall, resulting in completely different shape.

Table 5: List of the optimization cases

Case	Description	Design variables	Constraints	Mesh level
1	Keeping the upper wall straight	y Coordinates FFD(3), Inlet total pressure	Inlet Rey. number, 1.8<AR<4	L1

2	Optimization of the upper wall	x,y Coordinates FFD(2), y Coordinates FFD(3), Inlet total pressure	Inlet Rey. number, 1.8<AR<4	L1
3	Starting from a deformed geometry	x,y Coordinates FFD(2), y Coordinates FFD(3), Inlet total pressure	Inlet Rey. number, 1.8<AR<4	L1

D. Shape optimization to find the best straight wall diffuser

Before varying the upper wall profile in order to obtain a diffuser with an improved pressure recovery performance, it is interesting to know (and also compare to other …) what is the best straight wall diffuser? For this purpose, only the outlet area section (length in 2D) is changeable, and it is done by moving the FFD-3 top control points in y-direction only, and in range of $1.8 < AR < 4$, while the baseline configuration has AR=1.8. The recovery pressure coefficient, inlet Reynolds number and outlet static pressure are plotted (see Figure 2) against the optimization design iterations number. In this case $Cp = 0.636$ was obtained, which is an improvement of 23% compared to the baseline configuration. The optimized straight wall diffuser is characterized by $AR = 2.03$, and the upper wall profiles are shown in Figure 4. The optimized results were obtained after 20 design iterations.

The streamlines Mach number distribution for the baseline configuration (left figure) and the optimized straight-wall diffuser (right) is presented in Figure 3. The flow converges to a density residual of 10^{-10} and the adjoint equation convergence was set also to 10^{-10}. The optimality convergence tolerance of SLSQP optimization algorithm is typically 10^{-6} or less. The values of Cp and AR for the optimized straight-wall diffuser compares well with those reported by other published results [26].

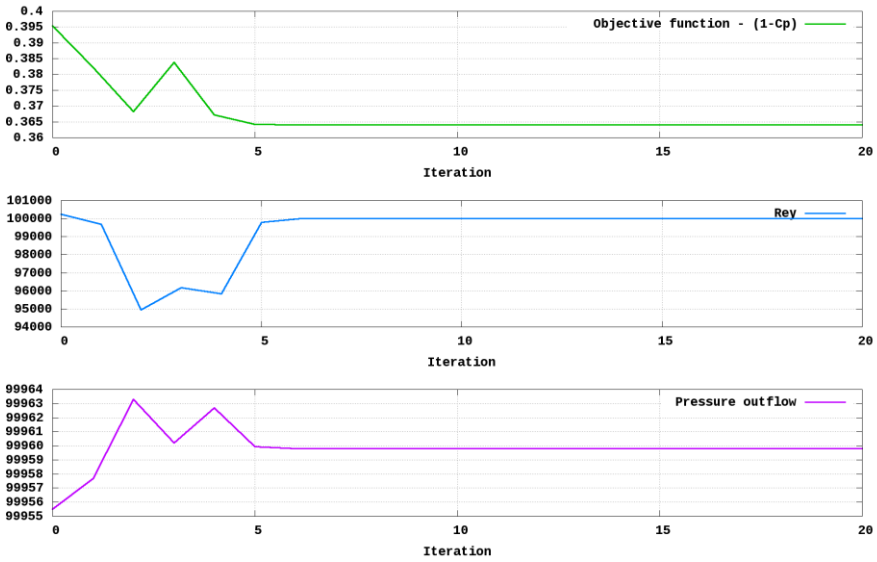

Figure 2: Convergence history of the pressure recovery coefficient, inlet Reynolds number and outlet static pressure for the straight wall configuration. The mesh level is L1.

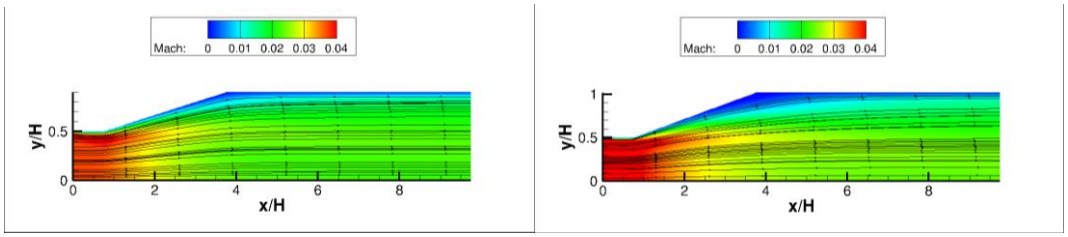

Figure 3: Mach number distribution while chnaging the outlet section area. Left: baseline configuration, right: optimized straight-wall diffuser with L/H=3, Rey=100K.

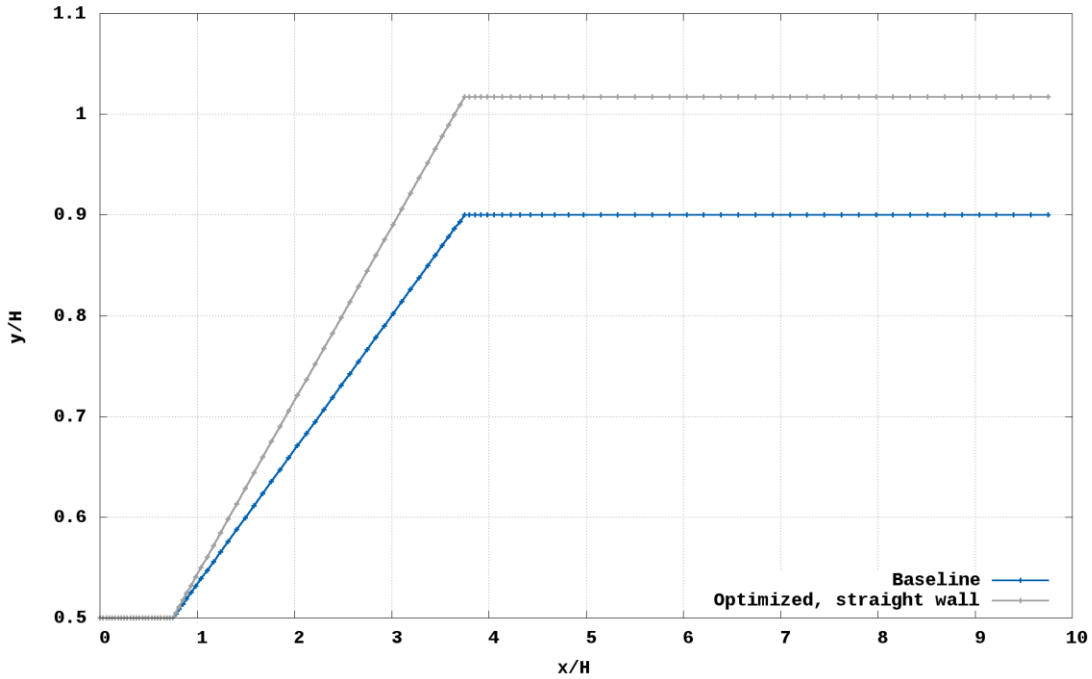

Figure 4: : Comparison of the diffuser upper wall profile of the base line geometry (blue) and the optimized configuration while starting from baseline (gray) and keeping the upper wall straight.

E. Diffuser's upper wall aerodynamic shape optimization

In the previous study only the area ratio was changed and the upper wall shape was kept fixed. This section presents a challenging aerodynamic optimization process by optimizing the upper wall shape, including the area ratio which is changeable in the range $1.8 < AR < 4$. This is done by using the outlet static pressure as a design variable in order to indirectly control the inlet Rey number, which is a constraint. So, the current study offers two important insights into the diffuser optimization methodology. First, it describes an alternative approach applying a constant mass flow rate boundary condition, if this kind of BC condition is not exist in the CFD software framework. Secondly, it offers some important insights into the effect of the area ratio on the performance of diffuser.

This optimization process repeated four times with different number of control points, in order to examine various design options. Table 6 summarizes the Cp values obtained with different control points. It is interesting to see that increasing the number of control points result in an improved pressure recovery coefficient. The optimum diffuser profile has a higher area ratio than the best straight walled diffuser and also produced a larger pressure rise. The Mach number streamline distribution is presented in Figure 5 for the optimized configuration. One can

observe the increased separation extent due to the sharp ending profile, compared to the baseline configuration. It is interesting to see that in the baseline configuration as well as the optimized one, the flow stays tight at the initial part of the diffuser but separates downstream forming a recirculation region.
Convergence is reached within 1189 seconds using 4 processors (for mesh level L0, and 24 control points), with 23 calls to the objective function and 19 calls to the sensitivity analysis function. Figure 6-Figure 7 presents the convergence history of $(1 - Cp)$, outlet static pressure and inlet Rey number for four simulations characterized with different number of control points. It takes more than 30 design iterations to reach convergence for the optimal diffuser. Again, the main computational effort here is for satisfying the required inlet Rey number constraint. A comparison of the upper wall profile between the optimized configuration and the baseline straight wall is presented in Figure 8, computed with 24 control points. The area ratio of the optimized diffuser is increased from 1.8 to 2.45 and it results in a lower static pressure which is the main driver for the mass flow rate through the diffuser.

Table 6: Values of pressure recovery with different number of control points (ncp)

ncp	ndv	Cp	AR
3	8	0.675	2.30
6	20	0.688	2.41
12	44	0.696	2.53
24	92	0.699	**2.45**

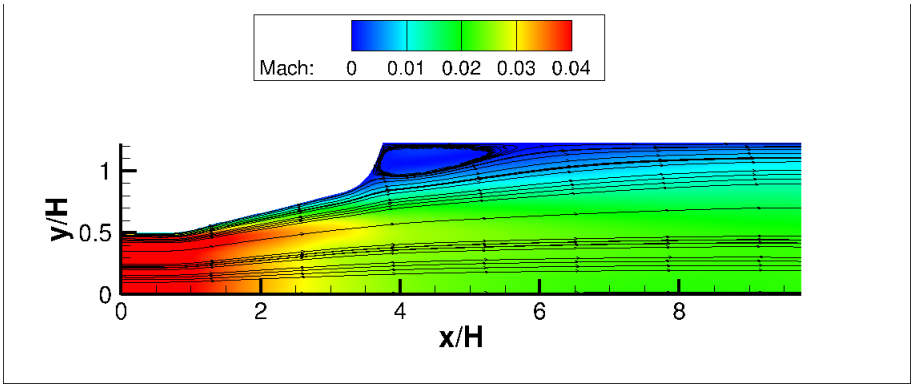

Figure 5: Mach number distribution while changing the upper wall and outlet section area.

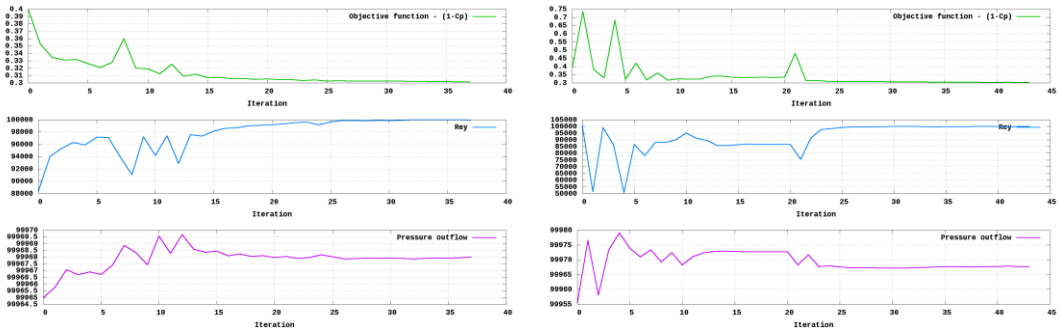

Figure 6: Convergence history of the recovery pressure coefficient, inlet Reynolds number and outlet static pressure for case 2 configuration. Results with mesh level L1, using 24 control points (left figure) and 12 control points (right figure).

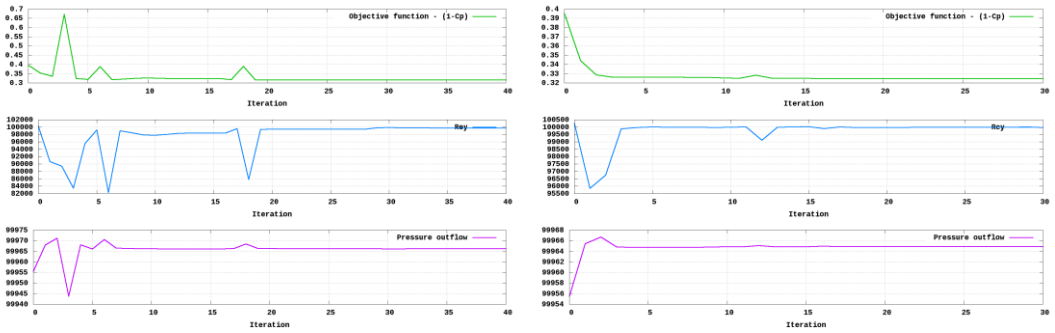

Figure 7: Convergence history of the recovery pressure coefficient, inlet Reynolds number and outlet static pressure for case 2 configuration. Results with mesh level L1, using 6 control points (left figure) and 3 control points (right figure).

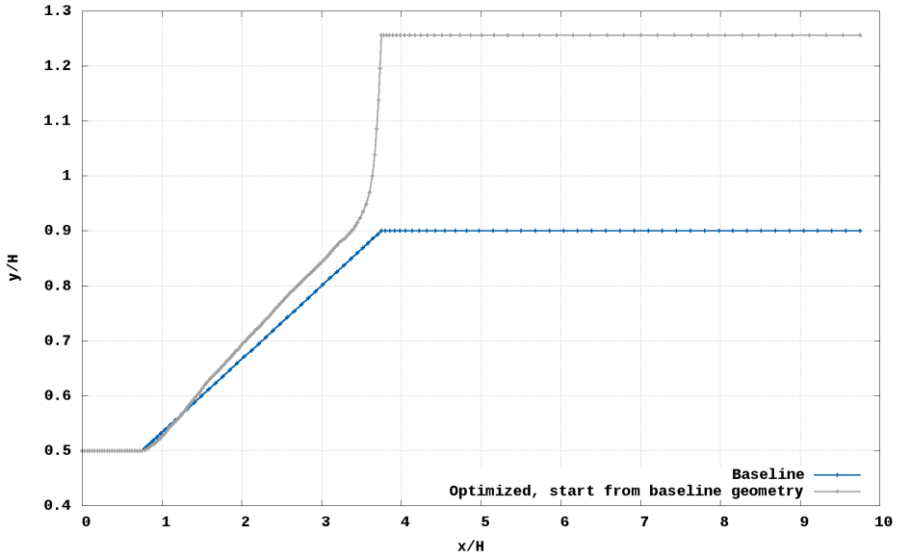

Figure 8: Comparison of the diffuser upper wall profile of the base line geometry (blue) and the optimized configuration (while starting from baseline (gray).

F. Optimizing the upper wall shape while starting from a deformed geometry

In this section the multi-modality of the diffuser shape optimization described in the previous section is explored by repeating the same optimization process (as the previous case) while starting from a deformed geometry. It is impossible to prove that the global optimum diffuser is found, but in order to verify that the problem is not multimodal a reasonable effort must be made to look for another optimal designs by starting from different (perturbed or deformed) geometry.

The baseline geometry is deformed by using Sculptor commercial software, by perturbing the diffuser upper wall in x and y directions. In order to avoid any uncertainties relating to the grid convergence issue the same mesh topology is projected (mesh level L0) for the deformed geometry (see Figure 9). The initial deformed design is well reflected by the optimizer convergence behavior, although the RANS solution converged well to the tolerance defined, within 70 design iterations. As expected, the deformed diffuser initial design performed poorly($Cp = 0.568$).

This solution attempt includes 24 control points and after 40 design iterations Cp is increased to 0.6940, 18.1% higher than the initial deformed geometry. Compared to the optimized diffuser while starting from the baseline geometry, the pressure recovery is lower in 0.8% only.

Despite the rather poor initial design, and the anomalous shapes encountered during the optimization process, the gradients point in the right direction, and the upper wall is smoothed out and finally similar geometry is obtained (see Figure 11). It is clearly seen that there are still some small visible differences between the wall shapes. The increased number of design variables caused the optimizer to explore shapes with more curvature variation. This minor difference in the final optimized upper wall profiles, including the pressure recovery values, may also be an indication that the global optimum diffuser is obtained.

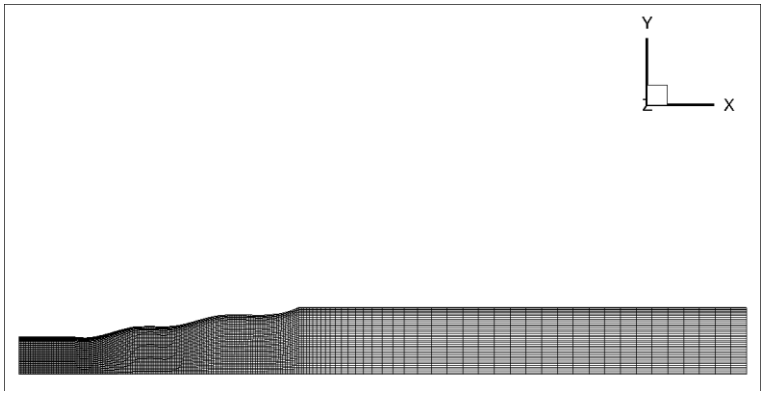

Figure 9: Initial deformed diffuser upper wall

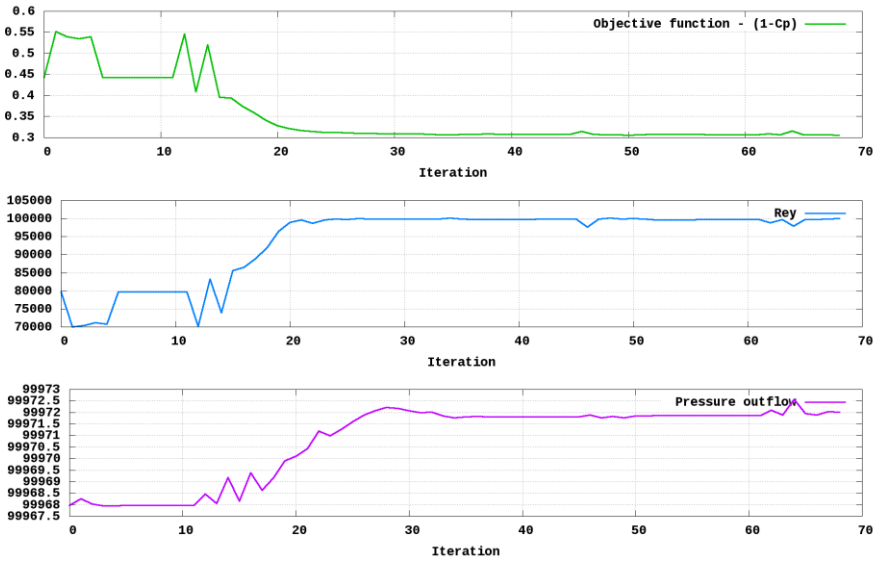

Figure 10: Convergence history of the recovery pressure coefficient, inlet Reynolds number and outlet static pressure for case 3 configuration. The mesh level is L0, using 24 control points.

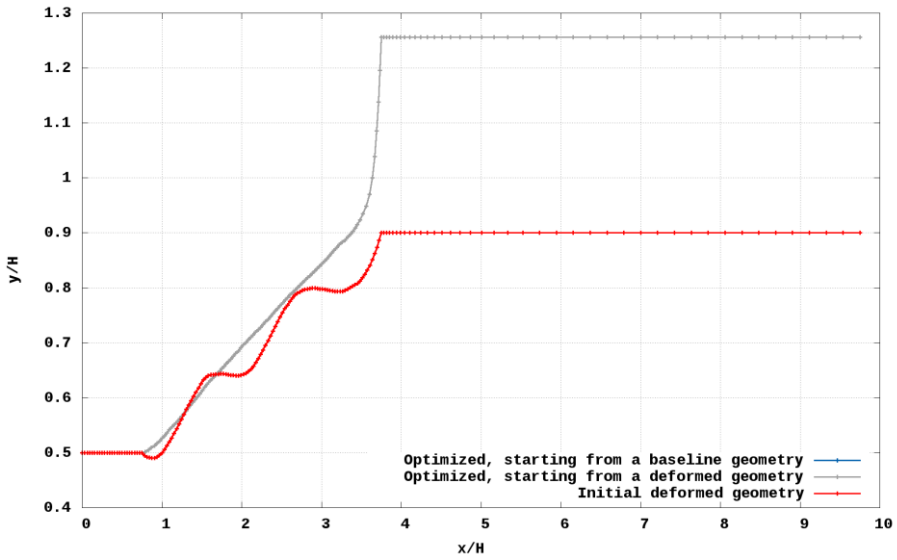

Figure 11: Comparison of the diffuser upper wall profile between the optimized configuration while starting from the base line geometry (blue) and the optimized configuration while starting from a deformed geometry (gray).

VI. Conclusions

This paper presents a modest experience to construct an aerodynamic optimization capabilities based on the gradient based algorithms together with an adjoint method that computes the required gradients efficiently. The main motivation for this research is analyzing the sensitivity and robustness of the flow solver, mesh warping method and the optimization algorithm to reduced sized problems, in a way that would fit the time and resources limitations exist in industrial applications. The effectiveness of the optimization process is demonstrated by benchmarking a 2D diffuser in a turbulent flow and constant inlet Reynolds number. Well converged results were obtained which are comparable to the results from previous work. Reasonably high pressure recovery are confirmed by comparing the optimized configurations with those of the straight wall diffuser design.

Also in this case, the robustness of the flow solver and mesh warping algorithm is demonstrated by starting the optimization process from a deformed geometry. In spite of the fact that this preferred starting condition might not be of interest for industrial applications, it definitely examines the robustness of the numerical method as well as the FFD parametrization method. The optimized shapes starting from straight wall and deformed wall are similar to each other except for minor differences, and the pressure recovery value is differ by 0.8% only.

[1] J. E. V. Peter and R. P. Dwight, "Numerical sensitivity analysis for aerodynamic optimization: A survey of approaches," *Computers and Fluids*, pp. 373-391, 2010.

[2] J. R. R. A. Martins and J. T. Hwang, "Review and unification of methods for computing derivatives of multidisciplinary computational models," *AIAA*, pp. 2582-2599, 2013.

[3] J. R. R. A. Martins, P. Sturdza and J. J. Alonso, "The complex-step derivative approximation," *ACM Transactions on Mathematical Software*, pp. 245-262, 2003.

[4] O. Pironneau, "On optimum design in fluid mechanics," *Journal of Fluid Mechanics*, vol. 64, pp. 97-110, 1974.

[5] A. Jameson, "Aerodynamic design via control theory," *Journal of scientific computing*, vol. 3, pp. 233-260, 1988.

[6] A. Jameson, "Computational algorithms for aerodynamic analysis and design," *Applied Numerical Mathematics,* pp. 383-422, 1993.

[7] D. A. Anderson, J. C. Tannehill and R. H. Pletcher, Computational Fluid Mechanics and Heat Transfer, New York: McGraw-Hill Book Company, 1984.

[8] L. C. L and H. R. J, "Solving Least Squares Problems," *Classics in Applied Mathematics, SIAM,* p. Volume 15, 1987.

[9] E. J. Nielsen and W. K. Anderson, "Aerodynamic design optimization on unstructured meshes using the Navier{Stokes equations,," *AIAA,* pp. 1411-1419, 1999.

[10] Z. L. G. K. W. K. J. R. R. A. M. S. Chen, "Aerodynamic shape optimization of the Common Research Model wing-body-tail con," *Journal of aircraft 53,* pp. 276-293, 2016.

[11] Z. L. Z. X. J. R. R. A. M. Y. Yu, "On the influence of optimization algorithm and starting design on wing aerodynamic shape optimization,," *Aerospace Science and Technology 75* , pp. 183-199, 2018.

[12] X. He, J. Li, C. A, Mader, A. Yildirim and J. R. R. A. Martins, "Robust aerodynamic shape optimization-from a circle to an airfoil," *Aerospace Science and Technology,* pp. 48-61, 2019.

[13] K. H. Svenningsen, J. I. Madsen, N. H. Hassing and W. H. G. Pauker, "Optimization of Flow Geometries Applying Quasi-Analytical Sensitivity Analysis," *Applied Mathematical Modelling,* vol. 20, pp. 214-224, 1996.

[14] J. I. O. N. Madsen and T. J. Condra, "Optimization of Straight, Two-Dimensional Diffusers by Wall Contouring and Guide Vane Insertion," in *World Congress of Structural and Multidisciplinary Optimization*, Buffalo, NY, USA, 1999.

[15] J. I. Madsen, W. Shyy and R. T. Haftka, "Response Surface Techniques for Diffuser Shape Optimization," *AIAA,* vol. 38, pp. 1512-1518, 2000.

[16] H. Çabuk and V. Modi, "Optimum Plane Diffusers in Laminar Flow," *Journal of Fluid Mechanics,* vol. 237, pp. 373-393, 1992.

[17] H. M. a. L. J. E. Lund, "Shape Design Optimization of Stationary Fluid-Structure Interaction Problems with Large Displacements and Turbulence," in *World Congress on Structural and Multidisciplinary Optimization*, Dalian, China, 2001.

[18] M. Dehghani, H. Ajam and S. Farahat, "Automated Diffuser Shape Optimization based on CFD Simulations and Surrogate Modeling," *Journal of Applied Fluid Mechanics,* vol. 9, pp. 2527-2535, 2016.

[19] J. R. R. A. Martins, K. W. K. Gaetan and T. Brooks, "Multidisciplinary Design Optimization of Aircraft Configurations - part2: High fidelity aerostructural optimization," in *Lecture series, Von Karman Institute for Fluid Dynamics*, Sint Genesius Rode, Belgium, 2016.

[20] E. K. G. S. J. a. A. J. van der Weide, "Unsteady Turbomachinery Computations Using Massively Parallel Platforms," in *44th AIAA Aerospace Sciences Metting and Exhibit*, 2006.

[21] A. S. W. a. T. E. Jameson, "Numerical Solution of the Euler equations by Finite Volume Methods Using Runge Kutta Stepping Schemes," in *14th AIAA, Fluid and Plasma Dynamics Coneference*, 1981.

[22] G. K. W. Kenway, G. J. Kennedy and J. R. R. A. Martines, "A CAD-free Approach to High Fidelity Aerostructural Optimization," in *13th AIAA/ISSMO Multidisciplinary Analysis Optimization Conference*, Fort Worth, 2010.

[23] R. E. Perez, P. W. Jansen and J. R. R. A. Martins, "A Python-based object-oriented framework for nonlinear contrained optimization, Structural and Multidisciplinary Optimization," 2012.

[24] D. Kraft, "A software package for sequential quadratic programming," DLR German Aerospace Center, 1988.

[25] P. J. Roache, K. Ghia and F. White, "Editorial Policy Statement on the Control of Numerical accuracy," *ASME Journal of Fluids Engineering*, p. 2, 1986.

[26] B. Djebedjian, "Two-Dimensional Diffuser Shape Optimization," in *International Mechanical Engineering Conference*, Kuwait, 2004.